Alfvén wave dispersion behavior in single- and multi-component plasmas

K Rahbarnia,[1,2,*] S Ullrich,[1] K Sauer,[3] O Grulke,[1,2] and T Klinger[1,2]

[1] *MPI for Plasma Physics, EURATOM Association, 17491 Greifswald, Germany*

[2] *Ernst-Moritz-Arndt-University, Greifswald, Germany*

[3] *University of Alberta - Edmonton, Alberta, Canada*

Abstract

Dispersion relations of driven Alfvén waves (AWs) are measured in single- and multi-component plasmas consisting of mixtures of argon, helium and oxygen in a magnetized linear cylindrical plasma device VINETA [C. Franck, O. Grulke and T. Klinger, Phys. Plasmas **9**(8), 3254 (2002)]. The decomposition of the measured 3D-magnetic field fluctuations and the corresponding parallel current pattern reveals that the wave field is a superposition of L- and R-wave components. The dispersion relation measurements agree well with calculations based on a multi-fluid Hall-MHD model if the plasma resistivity is correctly taken into account.

Keywords: Alfvén wave, dispersion relation, multi-component plasma, resistive Hall-MHD

*Electronic address: Kian.Rahbarnia@ipp.mpg.de

I. INTRODUCTION AND BASICS

In many astrophysical and laboratory plasmas more than a single ion species is present. In a multi-species plasma due to the occurrence of multiple resonances and cut-offs [1], the propagation of Alfvén waves [2] (AWs) is strongly affected. The resulting dispersion behavior is directly related to heat and energy transport in magnetized plasmas [3]. This is observed in laboratory [4–7] and fusion devices [8, 9] as well as in space plasmas, e.g., the solar atmosphere [10] or during the interaction between the solar wind with the cusp regions of the terrestrial magnetoshere [11]. AWs are responsible for heating of the solar corona [12] and acceleration of the solar wind [13, 14] by transferring energy from the sun's photosphere to the chromosphere in so-called flux tubes [15]. The interaction of the solar wind with cometary plasmas is determined by differently charged ions and dust grains [16–18] such that a multi-component plasma approach is needed to study the dynamics of instabilities (for example the firehose-instability [19, 20]). Collisions between different ion species can lead to a strong damping of the propagating waves [21, 22], as observed in interstellar clouds [23].

The aim of the present work is the measurement of AW dispersion relations in single- and multi-component plasmas in a well-controlled laboratory device, which allows one to study the dynamics of driven electromagnetic waves over a broad range of plasma parameters. The low-temperature discharge plasmas are accessible with probes in the entire plasma volume and the wave fields can be recorded with high resolution in space and time. We compare the experimental results with numerical calculations based on a multi-fluid Hall-MHD model including perpendicular resistivity. Together with Maxwell's equations, a plane wave ansatz leads to the dispersion equation in a cold uniform plasma [24]:

$$\omega^2 - k^2c^2 - \sum_j \frac{\omega\omega_{p,j}^2}{(\omega + i\nu) \pm \omega_{c,j}} = 0\,, \tag{1}$$

where c denotes the speed of light, ν the collision frequency and $\omega_{p,j}$ the plasma frequency. $\omega_{c,j} = q_j B_z/m_j$ is the cyclotron frequency of the particle species labeled j with the mass m_j and charge q_j. The ambient magnetic field is denoted with B. Eq. (1) holds for waves propagating parallel to the magnetic field and the $\pm$ sign stands for right-hand and left-hand circular polarized waves, respectively. The same result for the dispersion relation in a cold uniform plasma is obtained from a kinetic approach [25].

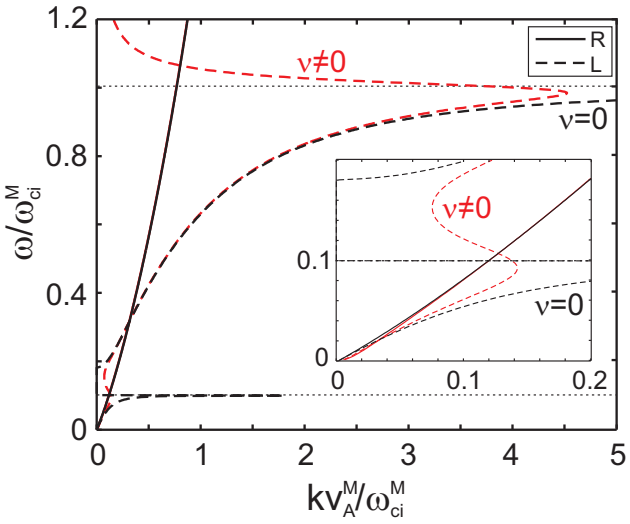

FIG. 1: (Color online) L-wave (dashed line) and R-wave (solid line) dispersion relations of a positive-positive ion plasma including ($\nu \neq 0$, red lines) and excluding ($\nu = 0$, black lines) collisions.

Fig. 1 shows an example of a L-wave (dashed line) and R-wave (solid line) dispersion relation achieved from Eq. (1) in a positive-positive ion plasma (helium (90 %) + argon (10 %), enlarged for lower frequencies) with ($\nu \neq 0$, red lines) and without ($\nu = 0$, black lines) including collsional effects. The normalizations $\omega' = \omega/\omega_{ci}^M$ and $k' = k(\omega)v_A^M/\omega_{ci}^M$ are made, where ω_{ci}^M and v_A^M are the ion cyclotron frequency and the Alfvén speed of the majority species. The L-wave has resonances at ω_{ci}^m (ion cyclotron frequency of the minority species) and ω_{ci}^M, which are less pronounced in the case of finite collisionality ($\nu \neq 0$). In a collisionless case ($\nu = 0$) the cutoff frequency ω_{co} of the L-wave ($k \to 0$ in Eq. (1) for $\omega \ll \omega_{ce}$, electron cyclotron frequency) is given by

$$\omega_{co} = \frac{n_M \omega_{ci}^m + n_m \omega_{ci}^M}{n}, \tag{2}$$

with $n = n_M + n_m$ being the plasma density, n_M and n_m being the density of the majority and minority ion species, respectively. ω_{co} is mainly determined by the ion cyclotron frequency of the minority species weighted with the ion density of the majority species. In the presence of collisions ($\nu \neq 0$) the wave vector k has a finite value at ω_{co} of the L-wave. These theoretical predictions are confirmed in the experiment, which is discussed in section IV. For $\omega \ll \omega_{ce}$ a significant influence of collisions on the R-wave propagation cannot be seen. The R-wave resonance at ω_{ce} is not shown in Fig. 1.

The present paper is organized as follows: After a description of the experimental setup in

section II, the AW dispersion measurements in single-component plasmas are discussed and the parallel current pattern is compared to the model results (section III). Subsequently the dispersion behavior of AWs in different two-ion species plasmas is studied in detail (section IV). The results are summarized in section V.

II. EXPERIMENTAL SETUP

The experiments are performed in the low-temperature plasma of the linear cylindrical plasma device VINETA (Fig. 2). The vacuum vessel has a total length of 4.5 m with a diameter of 0.4 m. It is immersed in a set of 36 magnetic field coils that generates a homogeneous magnetic field $B_z \leq 100\,\mathrm{mT}$. The working gases are argon, helium and oxygen. Steady-state plasma discharges are created by a standard helicon antenna [27, 28] operated at one end of the machine. The electron density and temperature profiles are measured by swept Langmuir probes. The profiles are peaked in the center and have a diameter of about 0.1 m [29]. Tab. I summarizes typical operation and plasma parameters for argon plasmas. The high collisionality has of course a strong effect on the AW dispersion behavior, especially when the AW frequency approaches the resonance at ω_{ci} [31]. Collisions are taken into account in the theoretical analysis to directly compare the model results to the experimental findings. In oxygen discharges, the negative ion density n_{O^-} is measured by laser-induced photo detachment [32]. An electronegativity of typically $\alpha = n_{O^-}/n_e \geq 1$ is found.

Electromagnetic waves are excited by an insulated Helmholtz coil in the plasma center oriented to produce a magnetic field perturbation mainly in y-direction. Each loop has 4 windings ($\phi = 3.5\,\mathrm{cm}$, distance of the loops 3.5 cm). Alternating currents up to 50 A are driven corresponding to a perpendicular magnetic perturbation of $B_y/B_z \approx 5\,\%$. The excitation geometry is not polarization selective. The magnetic wave field is measured with highly sensitive 3D-magnetic induction probes, which were calibrated in a test field. The miniaturized probe (length 18 mm, height 10 mm) consists of 1000 windings in each direction (B_x, B_y, B_z). It is shielded against electrostatic pickup and a temperature sensor in the head of the probe prevents overheating during plasma operation. A network of LC-absorption circuits suppresses the RF-frequency of the helicon source 13.56 MHz (attenuation -95 dB) and the harmonic 27.12 MHz (attenuation -69 dB). A set of low-noise differential amplifiers (type THAT1512) amplify the AW fluctuation signal by 60 dB. The lowest detection level

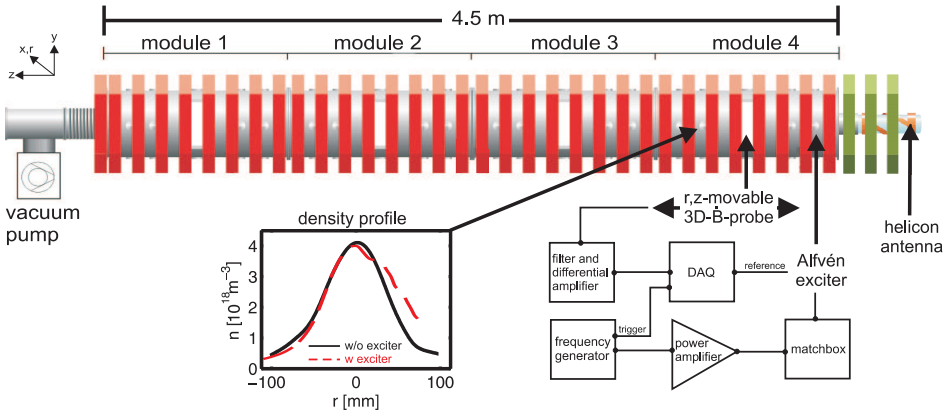

FIG. 2: (Color online) The **V**ersatile **I**nstrument for studies on **N**onlinearity, **E**lectromagnetism, **T**urbulence and **A**pplications VINETA [26] with a sketch of the exciter and detector setup including radial density profiles with (dashed line) and without exciter (solid line) inside the plasma.

is in the range of $B_{low} \approx 10\,\mathrm{nT}$. A detailed description of the Helmholtz coil exciter and 3D-magnetic probe design is topic of a separate publication [33]. Due to the miniaturization the influence of the exciter and detector system on the plasma profile is kept small. The central plasma depletion due to the presence of the exciter inside the plasma (Fig. 2, radial density profile with exciter, dashed line) is negligible.

III. ALFVÉN WAVES IN SINGLE-COMPONENT PLASMAS

In Fig. 3a the space-time evolution of the y-component of the magnetic field fluctuations B_y along the z-axis in an Argon plasma is shown. The Helmholtz-exciter is driven at a fixed frequency $f_{ex} = 23\,\mathrm{kHz}$ well below the ion cyclotron frequency $f_{ex}/f_{ci} = 0.79$. To avoid near field effects, the measurement starting position has a distance of 350 mm from the exciter. The phase fronts measured in the plasma center clearly show the stripe pattern of a propagating electromagnetic wave (Fig. 3a) with a phase velocity of $v_{ph} = 1.69 \cdot 10^5\,\mathrm{m/s} = 1.27\,v_A$. The wave is strongly damped with a damping lengths of $\lambda_d = 0.6\,\mathrm{m}$. For $f = 23\,\mathrm{kHz}$ the measured wave length is $\lambda = 7.3\,\mathrm{m}$, which is a typical Alfvén wave length also found previous work [6]. By driving the exciter at frequencies in the range $f_{ex} = 0 - 25\,\mathrm{kHz}$ (always well below f_{ci}) the dispersion relation of the propagating wave is obtained (Fig. 3b). For frequencies $f < 10\,\mathrm{kHz}$ drift wave instabilities [34] interact with the excited wave and lead to strong fluctuations of the phase velocity. In the considered low-frequency regime the

TABLE I: Typical operation and plasma parameters in argon plasmas. The ion temperature is taken from Ref. [30]. The ionization degree χ is estimated by $\chi = 100 \cdot n_e/(pV/k_bT)$ with $T = 300\,\mathrm{K}$, $V = 0.57\,\mathrm{m}^3$ vessel volume, k_B Boltzmann constant.

Parameter	Typical value
Working gas pressure p	$0.1\,\mathrm{Pa}$
RF-frequency f_{RF}	$13.56\,\mathrm{MHz}$
RF-power P	$4\,\mathrm{kW}$
Magnetic field B_z	$77\,\mathrm{mT}$
Ionization degree χ	$< 35\,\%$
Density n_e	$4 \cdot 10^{18}\,\mathrm{m}^{-3}$
Electron temperature T_e	$2\,\mathrm{eV}$
Ion temperature T_i	$0.2\,\mathrm{eV}$
Alfvén speed v_A	$1.33 \cdot 10^5\,\mathrm{m/s}$
Ion cyclotron resonance frequency f_{ci}	$29\,\mathrm{kHz}$
Ion-neutral collision frequency ν_{in}	$16\,\mathrm{kHz}$
Electron-ion collision frequency ν_{ei}	$5.7 \cdot 10^4\,\mathrm{kHz}$

phase velocity is a constant and the linear best fit yields $v_A^{fit} = 1.51 \cdot 10^5\,\mathrm{m/s} = 1.14\,v_A$, which agrees well with the Alfvén speed (with $v_A = B_z/\sqrt{\mu_0 m_i n_e}$). For different background magnetic field, density or ion species in single-component plasmas fully consistent findings were reported elsewhere [35].

Wave polarization

Due to the fact that the excitation scheme is not polarization selective, both left-hand (L) and right-hand (R) circular polarized waves are excited. The detailed analysis of the measured parallel current pattern in the azimuthal xy-plane yields that the observed wave field is actually a superposition of L-wave and R-wave that propagate simultaneously in the plasma.

The parallel current density j_z is obtained from Ampères law as $j_z = \partial b_x/\partial y - \partial b_y/\partial x$. Fig. 4a (first row) shows measurements of the current density $j_z(x, y, t)$ in the azimuthal

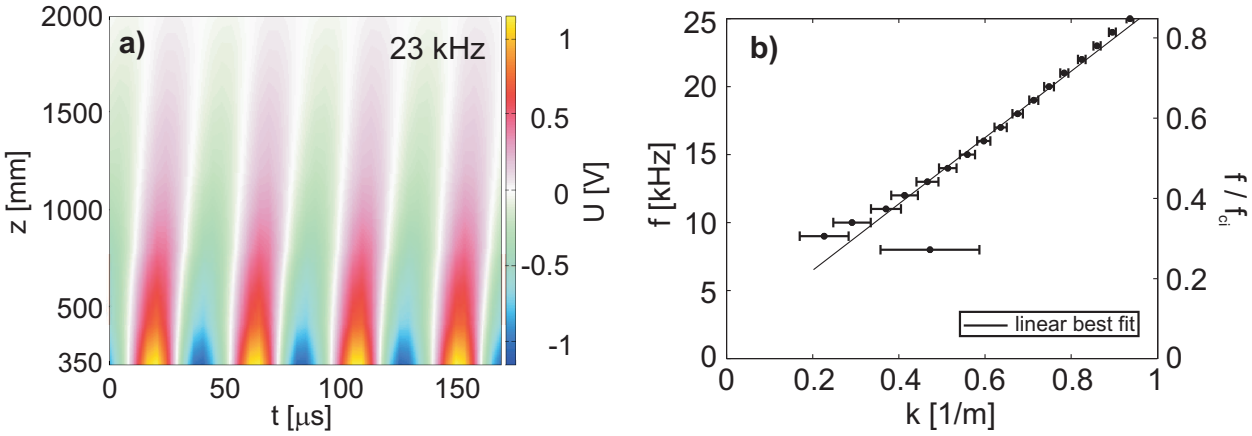

FIG. 3: (Color online) (a) Color-coded plot of the spatio-temporal evolution of B_y measured in the plasma center in an Ar discharge. (b) Measurement of the dispersion relation for a frequency range well below f_{ci}. The solid line is a linear best fit.

plane at $z = 1201\,\mathrm{mm}$ in an Ar discharge. The exciter frequency is chosen to be close to the ion cyclotron frequency. Two antiparallel current filaments are observed that flip sign after $17\,\mu\mathrm{s}$. A relatively complex intermediate current pattern occurs at $t = 8.5\,\mu\mathrm{s}$. For the interpretation of the data we assume that the space-time evolution of j_z can be reconstructed by a decomposition in L-wave and R-wave components. This is in fact the case: After transforming the measured current density into polar coordinates, left-hand and right-hand circular polarized parts are extracted by Fourier transform. They are distinguished by different mode numbers. Two dominant $m = \pm 1$ modes are found, where $m = -1$ corresponds to the L-wave (Fig. 4c) and $m = +1$ to the R-wave (Fig. 4d). The $m = -1$ structure in Fig. 4c is more pronounced than the $m = +1$ structure in Fig. 4d, which indicates a dominating shear-AW component, as expected for driver frequencies below f_{ci}. The superposition of both structures is shown in Fig. 4b. It matches the measured current pattern (Fig. 4a) quite well and demonstrates that the intermediate state at $t = 8.5\,\mu\mathrm{s}$ is also a result of the superposition of the two $m = \pm 1$ modes. Since all higher mode numbers are neglected, the maximum fluctuation amplitude is $j_z = 4.9\,\mathrm{mA/cm^2}$, about 40% lower than the measured value $j_z = 7.7\,\mathrm{mA/cm^2}$.

For a model description of the spatial structure of the excited wave field, a standard Hall-MHD description is chosen [24]. Collisional effects are taken into account by including the

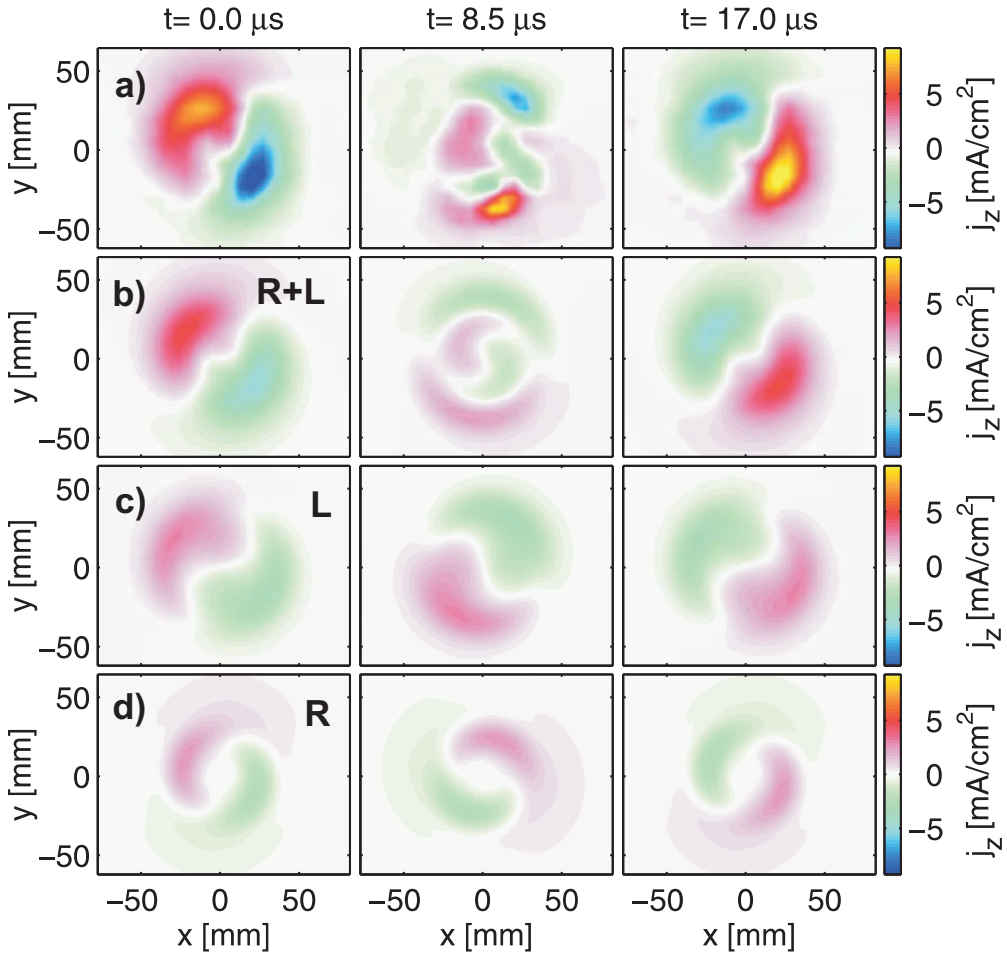

FIG. 4: (Color online) The color-coded plot of the parallel current density j_z (a) shows two antiparallel current filaments, which change sign after 17 μs. The superposition (b) of the decomposed components m=-1, L-wave (c) and m=1, R-wave (d) reflects the measurement.

perpendicular resistivity η in the generalized Ohm's law

$$\mathbf{E} + \mathbf{v} \times \mathbf{B} = \begin{pmatrix} \eta & 0 & 0 \\ 0 & \eta & 0 \\ 0 & 0 & 0 \end{pmatrix} \mathbf{j} + \frac{1}{en_e} \mathbf{j} \times \mathbf{B} \,. \tag{3}$$

Together with the equation of motion and Maxwell's equations, the space-time evolution of the fluctuating quantities magnetic field $\tilde{\mathbf{B}}$, electric field $\tilde{\mathbf{E}}$, plasma velocity $\tilde{\mathbf{v}}$ and current density $\tilde{\mathbf{j}}$ are obtained self-consistently using a plane wave ansatz. To account for the forced wave excitation, a magnetic field perturbation of $B_y = 200\,\mu$T perpendicular to the ambient magnetic field B_z is initialized at $z = 0$. The plasma density is assumed to be homogeneous. Fig. 5a shows the parallel current density of a shear-AW in the azimuthal plane. A spiral-

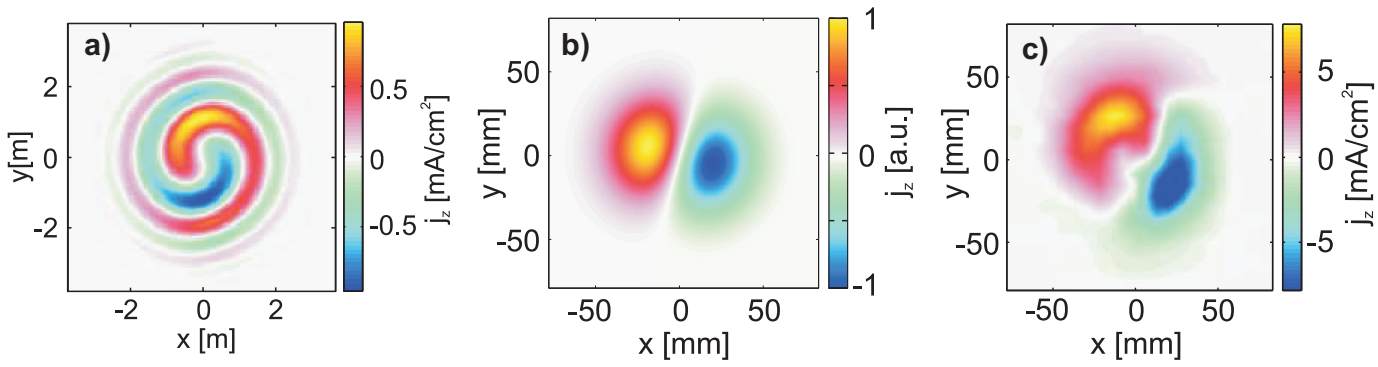

FIG. 5: (Color online) The parallel current pattern of a shear-AW predicted by a resistive Hall-MHD model for a homogeneous density profile has a spiral-like structure (a). Weighted with a Gaussian density profile similar to the experiment the resulting j_z (b) shows reasonable good agreement to the measured one in (c).

like structure of two intersecting antiparallel current filaments is found. The decrease of the amplitude at large radii indicates an increase of the damping at larger propagation angles with respect to the ambient magnetic field. This is a well-known property of shear-AWs, which propagate along the magnetic axes in so-called Alfvén cones [36]. However, the radial extent of the current pattern is on the order of meters, much larger than observed in experiment (Fig. 5c). This is a result of the assumed density profile. If the current density is weighted with a Gaussian density profile as found in the experiment [29] the radial extent of the current profile is dramatically reduced (Fig. 5b) and matches well the measurements (Fig. 5c).

We noted that the experimentally observed j_z-pattern consists of a superposition of L-wave ($m = -1$) and R-wave ($m = +1$) components, whereas the theoretical calculation consider the L-wave only. Nevertheless, a good agreement is found, which further supports the conclusion that the R-wave contribution is minor and the current pattern is dominated by the shear-AW.

IV. ALFVÉN WAVES IN MULTI-COMPONENT PLASMAS

The following section discusses the dispersion behavior of driven electromagnetic waves in multi-component plasmas, consisting of mixtures of argon, helium and oxygen in different concentration and composition. For a detailed comparison with Eq. (1), the measured wave

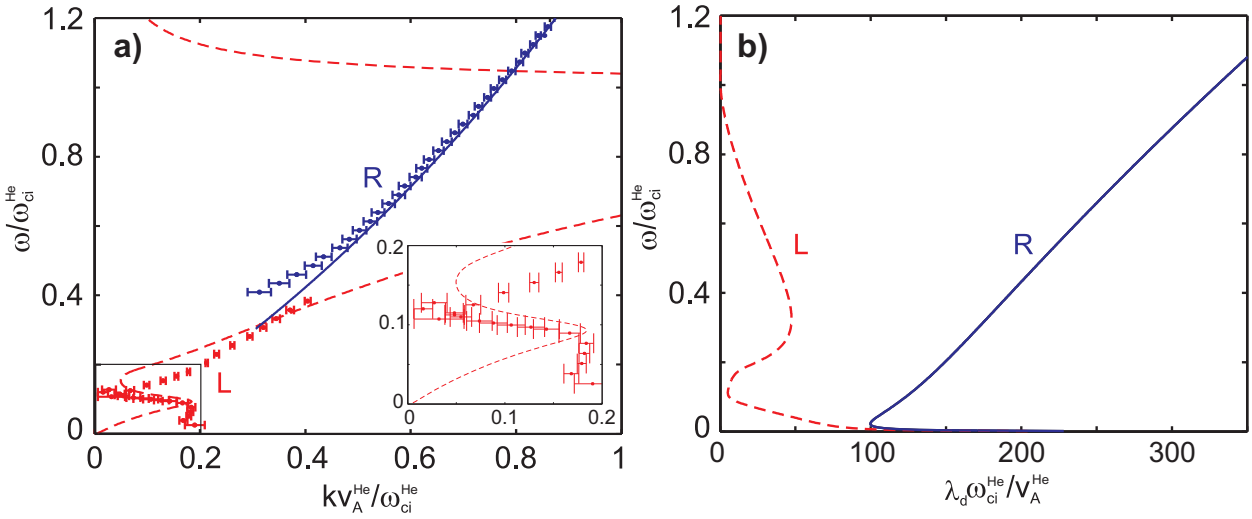

FIG. 6: (Color online) Dispersion relation (a) and damping length (b) in a two-ion species plasma [He (90%) + Ar (10%)]. The solution of Eq. (1) is shown as solid (R-wave) and dashed lines (L-wave).

field is decomposed into L-wave and R-wave components. The normalizations $\omega' = \omega/\omega_{ci}$, $k' = k(\omega)v_A/\omega_{ci}$ and $\lambda' = \lambda_d(\omega)\omega_{ci}/v_A$ are made, where $\lambda_d(\omega) = 1/\mathfrak{Im}[k(\omega)]$ is the damping length given by the imaginary part of the complex wave number $k(\omega) = \mathfrak{Re}[k(\omega)]+i\mathfrak{Im}[k(\omega)]$ (the ion cyclotron frequency ω_{ci} and the Alfvén speed v_A are taken for the majority species). The collision frequency and the density ratio of the involved ion species are used as fit parameters to model the experimental data. The resulting collision frequencies are on the order of the ion-neutral collision frequency found in the experiment ($\nu_{in}^{fit}/\nu_{in}^{exp} \approx 0.87$ for helium-argon plasma and $\nu_{in}^{fit}/\nu_{in}^{exp} \approx 5.91$ for argon-oxygen plasma). The obtained density ratios are $n_1^{fit} = n_{Ar}/n_{He} \approx 0.09$ and $n_2^{fit} = n_O/n_{Ar} \approx 0.83$, which agree well with the neutral gas pressure ratio used in the respective experiments ($n_1^{exp} = 0.1$, $n_2^{exp} = 0.8$). It is noted, that in helicon discharges the so-called neutral-pumping effect [37, 38] is suggested to cause a depletion of neutrals in the plasma center, which in the present study is not taken into account for the estimation of the neutral density.

Fig. 6a shows the measured dispersion relation in a positive-positive-ion plasma consisting of 90% helium and 10% argon (enlarged for lower frequencies). The experimental results are compared to the solution of Eq. (1), decomposed into R-wave (solid line) and L-wave (dashed line). In the presence of the second positive ion species, the excited wave shows an ion cyclotron resonance at $\omega/\omega_{ci}^{He} = 0.1$ (here is $\omega = \omega_{ci}^{Ar}$ the ion cyclotron frequency of argon),

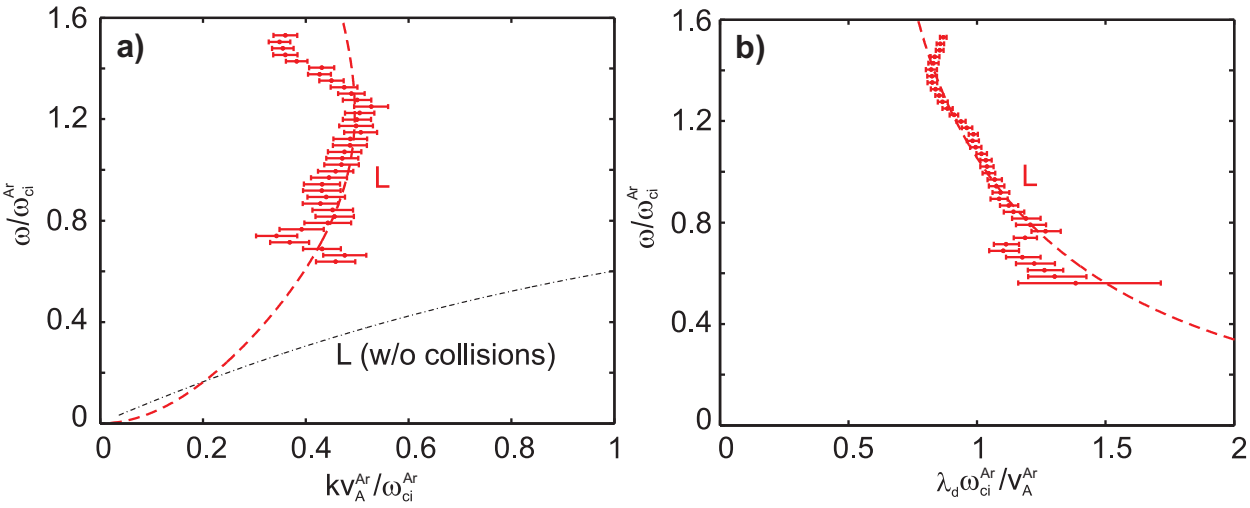

FIG. 7: (Color online) Dispersion relation (a) and damping length (b) of an excited shear-AW in an electronegative discharge [Ar (55%) + O (45%)]. The theoretical dispersion relation is shown as dashed line. The dash-doted line in (a) represents the model result if resistivity is excluded.

which is not very pronounced due to strong collisional damping of the L-wave indicated by a minimum of the damping length λ_d at $\omega/\omega_{ci}^{He} = 0.1$ (Fig. 6b). The measured L-wave dispersion follows qualitatively well the predicted relation up to frequencies $\omega/\omega_{ci}^{He} < 0.4$. For increasing frequencies the measured wave dispersion merges into the R-wave dispersion relation until the L-wave is completely damped. The increase of the damping of the L-wave becomes evident from the decreasing damping length for frequencies $\omega/\omega_{ci}^{He} > 0.4$ (Fig. 6b). Conversely the damping of the R-wave decreases as seen in the increasing damping length for $\omega/\omega_{ci}^{He} > 0.1$ (Fig. 6b). The upper cyclotron resonance at $\omega/\omega_{ci}^{He} = 1$ should have no influence on the propagating R-wave, which is confirmed by the measurement (Fig. 6a).

The measurement of the dispersion relation of shear-AWs in an electronegative plasma were done in a discharge with a mixture of argon (55%) and oxygen (45%). The result is shown in Fig. 7a. In a pure Ar discharge a single resonance at $\omega/\omega_{ci}^{Ar} = 1$ would be expected, whereas the measured dispersion relation shows a strongly damped wave with a maximum of $kv_A^{Ar}/\omega_{ci}^{Ar} = 0.52$ at $\omega/\omega_{ci}^{Ar} = 1.25$. The corresponding solutions of Eq. (1) (dashed line in Fig. 7) confirm the measurements. The deviation observed for frequencies $\omega/\omega_{ci}^{Ar} > 1.4$ might be due to boundary effects, which are not included in the theory. It is clear that the theory without resistivity does not apply to the experiment (dash-doted line in Fig. 7a).

V. SUMMARY

A combined setup of movable Langmuir probes and highly sensitive 3D-magnetic pick-up probes was installed on the linear plasma device VINETA. Via a Helmholtz coil pair, electromagnetic waves were driven in collisional single- and multi-component plasmas. The propagating wave field was measured with high spatial and temporal resolution. The excitation scheme is not polarization selective and the reconstructed 2D-parallel current pattern consists of a superposition of left-hand (L) and right-hand (R) circular polarized components. In a single-component plasma, for frequencies well below the ion cyclotron resonance frequency, the L-wave is clearly dominating, which is confirmed by a comparison with calculation results based on a resistive Hall-MHD model.

The dispersion relation of the excited waves was measured in single-component (Ar) and multi-component (Ar-O, He-Ar) plasmas. The experimental results agree over a wide range of frequencies with the theoretical dispersion relation, based on a multi-fluid resistive Hall-MHD model in a collisional cold uniform plasma. Due to the high collisionality, the driven wave is strongly damped. In case of the He-Ar discharge the L-wave is fully damped for frequencies $\omega/\omega_{ci}^{He} > 0.4$. The wave propagation is described by the R-wave dispersion relation.

ACKNOWLEDGMENTS

Part of this work has been done in the framework of the special collaboration research center of the German Research Foundation SFB-TR24, project A1.

REFERENCES

[1] T. X. Zhang and B. Li, Phys. Plasmas **11**(5), 2172 (2004).

[2] H. Alfvén, Nature, **150**, 405 (1942).

[3] E. J. Smith, M. Neugebauer, B. T. Tsurutani, A. Balogh, R. Forsyth and D. McComas, Adv. Space Res **20**(1), 55 (1997).

[4] D. Laveder, T. Passot and P. L. Sulem, Phys. Plasmas **9**(1), 293 (2002).

[5] F. J. Paoloni, Plasma Phys. **15**(6), 475 (1973).

[6] C. Watts and J. Hanna, Phys. Plasmas **11**(4), 1358 (2004).

[7] W. Gekelmann, S. Vincena and D. Leneman, Plasma Phys. Controll. Fusion **39**(5A), 101 (1997).

[8] G. Besson, A. De Chambrier, G. A. Collins, B. Joye, A. Lietti, J. B. Lister, J. M. Moret, S. Nowak, C. Simm and H. Weisen, Plasma Phys. Controll. Fusion **28**(9A), 1291 (1986).

[9] G. Gnavi, R. M. O. Galvão, F. T. Gratton and L. Gomberoff, Phys. Rev. E **54**(4), 4112 (1996).

[10] S. Tomczyk, S. W. Mclntosh, S. L. Keil, P. G. Judge, T. Shad, D. H. Seeley and J. Edmondson, Science **317**, 1192 (2007).

[11] D. Sundkvist, A. Vaivads, M. André, J. E. Wahlund, Y. Hobara, S. Joko, V. V. Krasnoselskikh, Y. V. Bogdanova, S. C. Buchert, N. Cornilleau-Wehrlin, A. Fazakerley, J. O. Hall, H. Rème and G. Stenberg, Ann. Geophys. **23**(3), 983 (2005).

[12] D. B. Jess, M. Mathiodakis, R. Erdélyi, P. J. Crockett, F. P. Keenan and D. J. Christian, Science **323**, 1582 (2009).

[13] B. De Pontieu, S. W. McIntosh, M. Carlsson, V. H. Hansteen, T. D. Tarbell, C. J. Schrijver, M. Title, R. A. Shine, S. Tsuneta, Y. Katsukawa, K. Ichimoto, Y. Suematsu, T. Shimizu and S. Nagata, Science **318**, 1574 (2007).

[14] A. Verdini and M. Velli, Astrophys. J. **662**, 669 (2007).

[15] H. Pecseli and O. Engvold, Solar Physics **194**, 73 (2000).

[16] M. P. Hertzberg, N. F. Cramer and S. V. Vladimirov, Phys. Rev. E **69**(056402), 2172 (2004).

[17] N. F. Cramer and S. V. Vladimirov, Phys. Plasmas **3**(12), 4740 (1996).

[18] M. Salimullah and M. Rosenberg, Phys. Lett. A (254), 347-350 (1999).

[19] B. Tsurutani, R. Thorne, E. Smith, J. Gosling, and H. Matsumoto , J. Geophys. Res. **92**(A10), 11074-11082 (1987).

[20] K. B. Quest and V. Shapiro, J. Geophys. Res. **101**(A11), 24457-24469 (1996).

[21] C. Uberoi, J. Plasma Phys. **52**, 215-221 (1994).

[22] C. Uberoi and A. Datta, Phys. Plasmas **5**(12), 4149-4155 (1998).

[23] W. Pilipp, T. W. Hartquest, O. Havness and G. E. Morfill, Astrophys. J. **314**, 341-351 (1987).

[24] N. F. Cramer, *The Physics of Alfvén Waves* (Wiley-VCH, Berlin, 2001) Chap. 2.

[25] S. P. Gary, *Theory of space plasma microinstabilities* (Cambridge University Press, Cambridge, 1993) Chap. 6.

[26] C. Franck, O. Grulke and T. Klinger, Phys. Plasmas **9**(8), 3254 (2002).

[27] F. F. Chen, *High density plasma sources* (Noyes Publications, New Jersey, 1995) Chap. 1.

[28] R. W. Boswell, Plasma Phys. Controll. Fusion **26**(10), 1147 (1984).

[29] C. Franck, O. Grulke and T. Klinger, Phys. Plasmas **10**(1), 323 (2003).

[30] A. Stark, O. Grulke and T. Klinger, AIP Conf. Proc., PLASMA 2005: Int. Conf. on Research and Applications of Plasmas; 3rd German-Polish Conf.on Plasma Diagnostics for Fusion and Applications; 5th French-Polish Seminar on Thermal Plasma in Space and Laboratory, Opole-Turawa, Poland, 6-9 September 2005, edited by M. J. Sadowski, M. Dudek, H.-J. Hartfuss, E. Pawelec, Vol. **812**(1), pp. 141-144.

[31] Y. Amagishi and M. Tanaka, Phys. Rev. Lett. **71**, 360 (1993).

[32] N. Sydorenko, O. Grulke, K. Matyash, R. Schneider, S. Ullrich and T. Klinger, Contrib. Plasma Phys. **49**(1), 27-35 (2009).

[33] S. Ullrich, K. Rahbarnia, O. Grulke and T. Klinger, to be published in Rev. Sci. Instrum.

[34] C. Schröder, O. Grulke, T. Klinger and V. Naulin, Phys. Plasmas **12**(042103) (2005).

[35] K. Rahbarnia, S. Ullrich, A. Stark, O. Grulke and T. Klinger, J. Plasma Fusion Res. SERIES **8**, pp. 0031-0034 (2008).

[36] W. Gekelman, D. Leneman, J. Maggs and S. Vincena, Phys. Plasmas **1**(12), 3775 (1994).

[37] J. Gilland, R. Breun and N. Hershkowitz, Plasma Sources Sci. Technol. **7**, 416-422 (1998)

[38] D.G. Miljak and F. F. Chen, Plasma Sources Sci. Technol. **7**, 537-549 (1998)